

Incorporation of fracture directions into 3D geostatistical methods for a rock fracture system

Katsuaki Koike · Chunxue Liu · Tomoji Sanga

Received: 6 October 2010 / Accepted: 3 September 2011 / Published online: 20 September 2011
© Springer-Verlag 2011

Abstract Simulating a rock fracture distribution is an important problem common to various fields in geosciences. This paper presents GEOFRAC, a geostatistical method to simulate a fracture distribution by incorporating the directions (strikes and dips) of the sampled fracture data into the simulation. Fracture locations are generated randomly following fracture densities assigned by a sequential Gaussian simulation. Fracture directions are transformed into an indicator set consisting of several binary (0 and 1) variables and the variables are compressed using the principal component analysis. Ordinary kriging is then employed to estimate the distributions of these principal values and the results are back-transformed into the coordinate system of the original indicator set. Fracture directions are generated randomly using their histograms within the defined directional interval. Finally, facets (fracture elements) are determined from the simulated locations and directions, and the fractures within the angle and distance tolerances are connected to form a fracture plane. From a case study of

applying GEOFRAC to the fracture data in Kikuma granite, southwest Japan, GEOFRAC was shown to be able to depict a plausible fracture system because the simulated directions corresponded well to those measured. Furthermore, the simulated fracture system was available to estimate the hydraulic conductivity of the study site, which was roughly in agreement with the average of hydraulic test results.

Keywords Fracture orientation · Fracture density · Principal component analysis · GEOFRAC · Granite · Hydraulic conductivity

Introduction

One of the most important rock properties is fractures that exist on every scale from micro- to mega-meters due to various genetic mechanisms such as cleavage, cooling, tensile, and shear. Fractures have been studied both in sciences for understanding tectonic history and geological structures and in engineering for characterizing hydraulic and mechanical properties of rock mass aimed at natural resources exploration, rock structure and storage constructions, and assessment on contaminant spread with groundwater flow. In both fields, correct imaging of the fracture system and a plausible 3D distribution model are indispensable and can contribute greatly to clarify fracture-related geo-phenomena and environments.

For pursuing more sophisticated fracture modeling, many methods have been proposed during the last four decades. At an early stage, the fracture network was modeled simply by three orthogonal families of infinite planes with constant or random spacing (Snow 1969). For the models of Poisson distributions of planes or lines in 2D, the distance of an infinite fracture plane from an arbitrary

Electronic supplementary material The online version of this article (doi:10.1007/s12665-011-1350-z) contains supplementary material, which is available to authorized users.

K. Koike (✉)
Department of Urban Management,
Graduate School of Engineering, Kyoto University,
Katsura C1, Kyoto 615-8540, Japan
e-mail: koike.katsuaki.5x@kyoto-u.ac.jp

C. Liu
School of Urban Management, Environment and Resources,
Yunnan University of Finance and Economics,
237, Longquan Rd., Kunming 650221, China

T. Sanga
Nikko Exploration and Development Co., Ltd.,
Toranomon 2-7-10, Tokyo 105-001, Japan

origin is defined to follow a Poisson process and its direction is also given randomly or in consideration of dominant fracture sets (Priest and Hudson 1976; Andersson et al. 1984; Andersson and Thunvik 1986). Fracture networks composed of infinite planes are generated by extending and improving the Poisson plane model (Dershowitz and Einstein 1988; Chilès 1988) or Boolean model (Long et al. 1985; Andersson and Dverstrop 1987; Rouleau and Gale 1987; Cacas et al. 1990). Geostatistical fracture modeling is proposed by Long and Billaux (1987) and uses variograms of fracture density variations for seeding fracture centers in 2D space. Applications of fractal methods to 3D modeling of naturally fractured rock masses and reservoirs are reviewed by Hewett (1994).

For fracture generation methods considering fracture distribution properties, the following references are noted. To simulate a heterogeneous generation process, Billaux et al. (1989) proposed a parent–daughter procedure to generate clusters of fractures in which a parent is a fictitious object composed of real objects: fractures. Clemo and Smith (1997) used a Levy flight process to build fractal networks conditioned on maps of fracture traces. Acuna and Yortsos (1995) adopted a randomized iteration procedure to generate a hierarchical fractal network, which can adjust its fractal dimension to that of observed fractures by a box-counting method. Riley (2004) suggested a statistical, rule-based method for generating fracture patterns. A more advanced method is an integrated conditional global optimization by Tran et al. (2006) in which representative properties such as direction, size, and aperture can be reflected.

In spite of the development of the above fracture modeling techniques, most techniques employ Gaussian or Poisson stochastic procedures and then, a realistic 3D modeling is difficult to perform from the observed fracture data along boreholes or on rock walls which are limited in number and location. Nuclear magnetic resonance (NMR) and X-ray computer tomography (CT) can visualize 3D fractures, but sample size and visible fractures are too limited to analogize a field-scale condition. In addition, sampling inadequacy causes “censoring bias” of fracture data in terms of length, quantity, and direction. Although several methods have been proposed to correct such bias (Terzaghi 1965; Heffer and Bevan 1990; Odling 1997; Mauldon et al. 2001), most are based on strict assumptions that are effective for specific problems and are not versatile.

Other properties cause difficulties in 3D fracture modeling: the fracture is not merely a geometrical feature but has multiple attributes such as aperture, filling minerals, roughness, and displacement; fractures form sets usually with dominant directions; fracture networks have hierarchical structure; and it is uncertain how the fractal model of fractures is to be applied for a wide range of fractures and for different attributes such as length, width, and direction.

As a geostatistical technique to partially overcome the above problems, this paper proposes GEOstatistical FRACture simulation method (GEOFRAC) that has merit in its extension to 3D modeling and suitable assignments of fracture density and directions. Namely, the primary aim of this paper is an application of geostatistics to model 3D fracture system and more particularly fracture orientations, and kriging of principal components similar to Suro-Pérez and Journel (1991) which is one of the key aspects of the proposed method. GEOFRAC is applied to the fracture data obtained by constructing petroleum storage tanks at a granite site.

Principle of GEOFRAC

At first, a fracture is supposed to be composed of connected fracture facets (fracture elements) which are stochastically simulated objects. In a similar manner to a usual fracture simulation, GEOFRAC approximates a facet to have a disk shape with definite direction (strike and dip) so the dimension of a fracture can be represented simply by a diameter. All the disks have the same size. However, by connecting multiple fracture disks that have similar directions and are closely located, one fracture can be formed with a slightly undulating surface and complicated edge shape. GEOFRAC consists of three main steps: (1) positioning of facet centers, (2) assignment of directions (strikes and dips), and (3) connection of facets to form fractures. Steps (1) and (2) follow the ideas of Koike et al. (2001) and Koike and Ichikawa (2006), but are revised for 3D simulation. One merit of GEOFRAC that simulates facets first is that a long fracture can be formed by identifying a set of connectable facets by post-processing instead of directly simulating long fractures. Fracture length distribution becomes possible by estimating through the simulation result.

Positioning of fracture centers

In the first step of fracture simulation, fracture locations are determined by their center points. This positioning is accomplished based on a fracture density map. As the simplest way by focusing on a geometrical aspect of fractures, fracture density is defined as the number or total area of fractures per unit volume in 3D, the number or total length of fractures per unit area on a trace map in 2D, and the number of fractures intersecting a scanline per unit length in 1D. GEOFRAC defines fracture density by the number of fracture centers per unit grid-cell. This center is a facet center, but not a true fracture center: as mentioned above. A fracture is supposed to be composed of several concatenated facets with similar directions. Fracture density is used to identify facets simulating a long fracture

plane. The density may be also biased, but it does not affect strongly this type of simulation.

After modeling of the experimental semivariogram [$\gamma(h)$ hereafter] of the fracture density data from field observations, the 3D distribution of the fracture density is simulated by sequential Gaussian simulation (SGS) (e.g., Deutsch and Journel 1998). The reason for using SGS is that it can overcome the problem in the density map from ordinary kriging (OK) in which the densities are strongly affected by the nearest data and many linear, unnatural boundaries of densities appear as shown in Koike et al. (2001). SGS can be used to reproduce or capture spatial statistics of sparse data, which is difficult to achieve by other estimation methods. A normal score transformation was applied to the SGS calculation.

The next step is generation of the same number of fracture centers in each grid-cell as that estimated by the fracture density for each grid-cell, and their locations are given using random numbers that follow a uniform distribution.

Assignment of fracture directions

It is a common geological phenomenon that fractures can be grouped into a few sets with almost the same directions, as seen in granitic rocks; fractures with similar directions are located closely and fractures form specific patterns such as conjugate sets under compressive stress. This means that the fracture directions are not randomly distributed but must have some spatially correlated structure. The key point of GEOFRAC is how this directional correlation can be incorporated into the fracture modeling to produce a plausible distribution.

Fracture direction can be represented by a strike and dip such as N50°E and 80°SE in the geological convention. To transform into the trigonometric expression by the right hand rule as shown in Fig. 1a, strike and dip are denoted as an angle α counted anticlockwise from the east (0–360°) and an angle β (0–90°), respectively, in which the dip direction is set on the right side of the strike. Following this rule, fractures striking NE/dipping NW and striking NW/dipping SW have 180° added to their strike angles as in Fig. 1b. For example, a strike/dip of N40°E/70°NW becomes $\alpha = 230^\circ/\beta = 70^\circ$ and that of N60°W/50°SW becomes $\alpha = 330^\circ/\beta = 50^\circ$. This definition of direction is for facilitating computer calculation and programming.

Firstly, the fractures are divided into different intervals in direction to simplify the expression and form regionalized random variables related to direction for spatial modeling. Figure 2 depicts examples of this type of division: 8 and 16 directional intervals in which α is divided equally by 45° increments; the 16 divisions consider the dispersion of dips and β is divided into gentle (0–45°) and steep (45–90°) angles. Fractures are classified into several sets generally

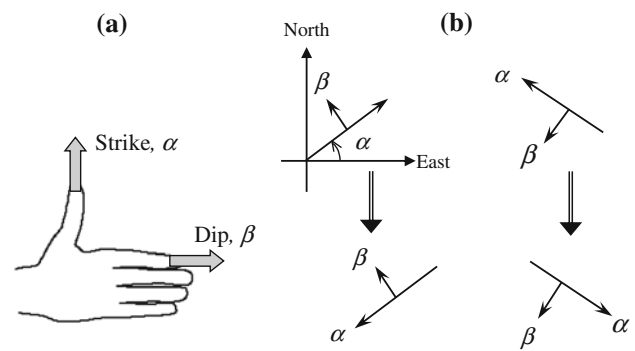


Fig. 1 Right hand rule for representing strike and dip directions of a fracture: **a** dip direction is set on the right side of the strike. By this rule, **b** fractures striking NE/dipping NW and striking NW/dipping SW have 180° added to their strike angles

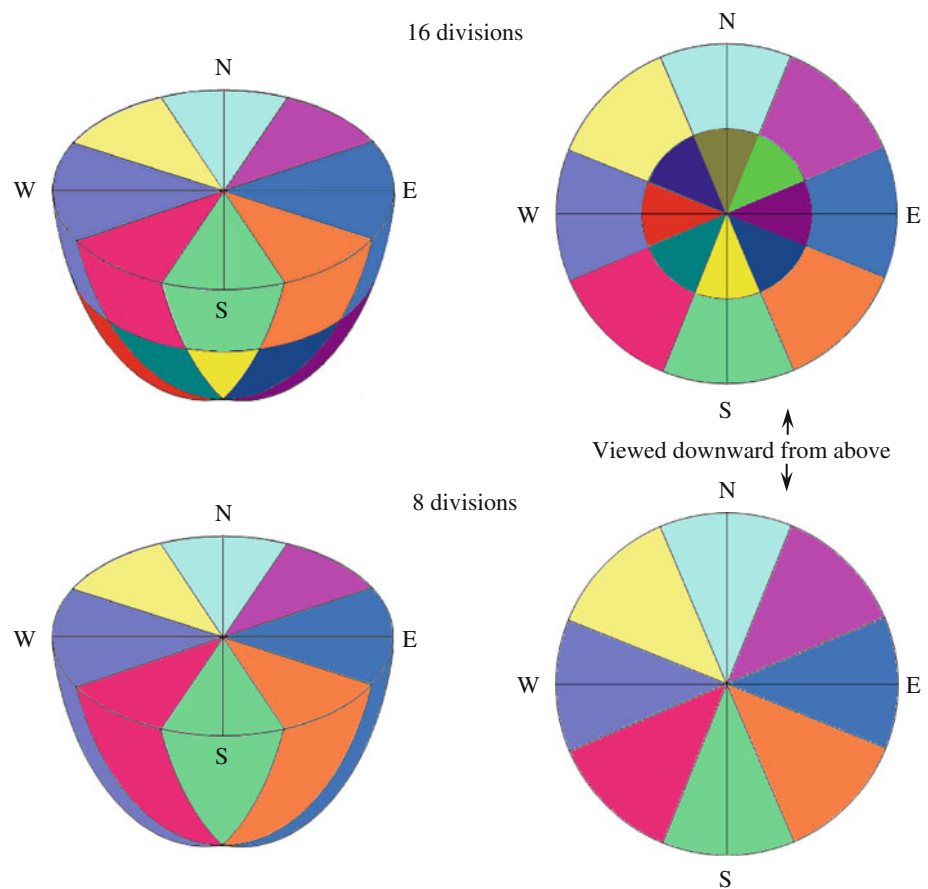
based on preferable orientations, types, and tectonic properties. However, the directional ranges tend to be different with the different sets. To consider the spatial dependence of similar and different fracture orientations simply, the above mechanical divisions were adopted. For each interval, a cumulative distribution function (CDF) of the direction is modeled using the sample data falling in the interval under an assumption that strike and dip are independent. Let the number of intervals be n and the fracture direction be transformed into an indicator set, (g_1, g_2, \dots, g_n) , that consists of n binary (1 or 0) data. Only the interval into which the α and β fall is given a value 1 and the other intervals are given values 0, e.g., $(0, 1, 0, \dots, 0, 0)$. A suitable n is selected by the criterion that the clouds of directions can be decomposed adequately and the spatial correlation structures of the intervals can be determined by variography.

For clarifying correlations of all the directional pairs, n $\gamma(h)$ s of the same interval and $n(n-1)/2$ cross-semivariograms ($\gamma_c(h)$ s) for different interval pairs are necessary in total. To reduce the amount of calculation, principal component analysis (PCA) was adopted, as similar to indicator principal component kriging method (Suro-Pérez and Journel 1991), and the data in a set were transformed into $n-1$ principal values; the n -th principal values become zero for the above indicator set. Therefore, only $n-1$ experimental $\gamma(h)$ s need to be calculated. Principal values are then given to the simulated fracture centers using OK or SGS. Cross-validation between the sample-data and calculation values and comparison of the resultant spatial models by OK and SGS are the criteria on selecting a method. The principal values are obtained from the linear combination of g_j with coefficients C_j by maximizing their variance.

$$\text{Var} \left\{ \sum_j^n C_j g_j \right\} \rightarrow \max, \quad \text{s.t.} \quad \sum_{j=1}^n (C_j)^2 = 1 \quad (1)$$

After the kriging estimates, the principal values are back-transformed into the original coordinate system of the

Fig. 2 Examples of the division of fractures into intervals of 8 and 16 directions in which the strikes are divided equally by 45° . For the 16 divisions, dips are further divided into gentle ($0\text{--}45^\circ$) and steep ($45\text{--}90^\circ$) angles



indicator set. The set is not composed of binary numbers but of positive decimal fractions such as (0.2, 0.3, 0.9, ..., 0.1, 0.05). From the set, the interval that has the largest value is selected (g_3 for this example set) as the most likely direction at the fracture center under the conditional estimation using nearby sample data. This selection method ignores the possibility that a fracture direction belongs to multiple intervals, but it requires no further assumptions. This is the reason for adopting the method. Finally, a direction (α and β) is given to the center by applying the Monte-Carlo method to the CDF in the interval. A combination of the estimation by OK and the simulation by Monte-Carlo is used to determine the direction as described later.

Connection of facets

Through the above two steps, center locations and directions of facets are determined. The next step is the connection of facets by the criteria of nearness of centers and similarity of directions. The following two criteria are compared; for both criteria, the distance between two fracture centers, l_c , is used and the threshold for l_c of connectable facets is denoted as l_t .

Connection considering fracture centers only

As shown in Fig. 3a, this criterion is based on the differences in strike and dip angles, α_d and β_d , between two facets. Two fractures are connected if all l_c , α_d , and β_d are smaller than their corresponding thresholds, l_t , α_t , and β_t .

Connection considering fracture planes

The second criterion uses the directional difference between two fracture planes. Here, a fracture plane is defined to have a finite size. By projecting the line connecting the centers onto the planes, two included angles, φ_1 and φ_2 , between the projected line and the connection line are measured. The connection criterion is that both φ_1 and φ_2 are smaller than the threshold φ_t and the l_c is shorter than l_t . This criterion has an advantage in that it can prevent echelon-type fractures which have similar directions but are distributed in parallel from being connected.

Isolated facets are expressed as having disk shapes with a constant diameter. After the connection, another important problem is how one plane can be approximated from more than two connected facets with slightly

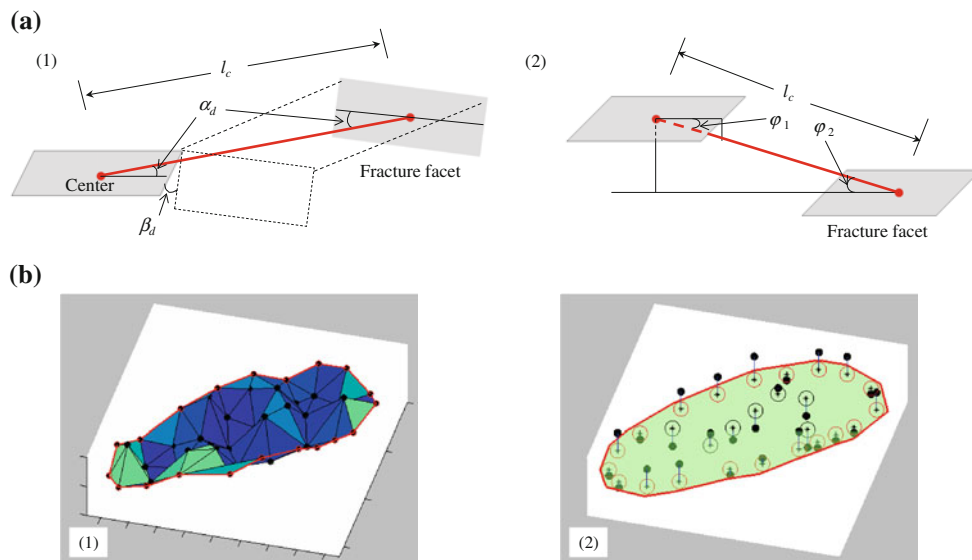
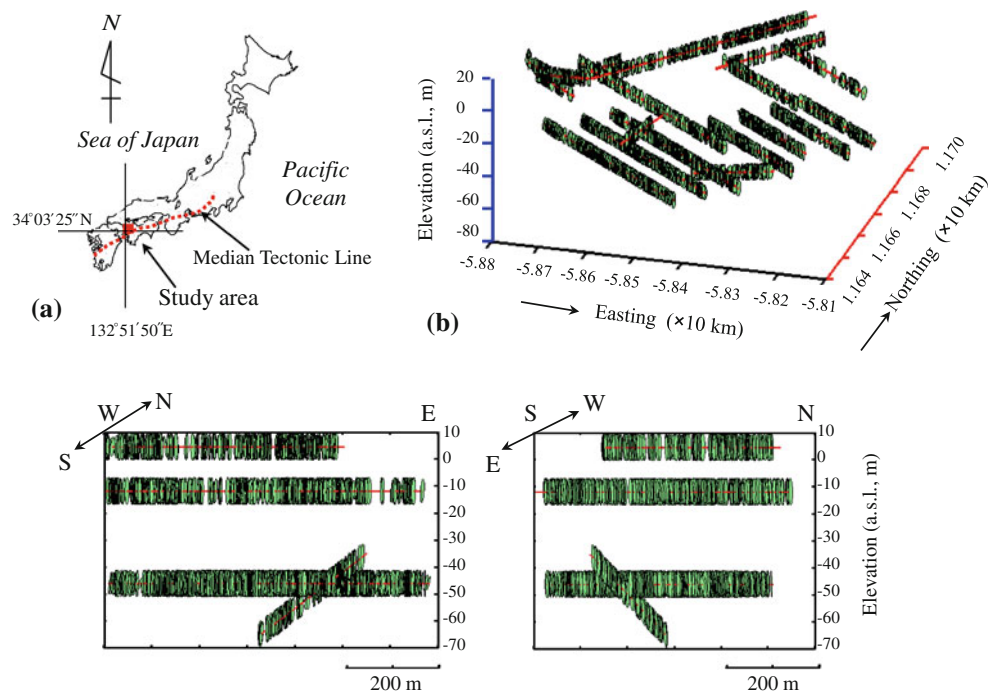


Fig. 3 a Two criteria for connecting two facets for which the distance between two fracture centers is denoted by l_c . Connection (1) considering fracture centers only is based on the differences in strike and dip angles, α_d and β_d , between two facets. Connection (2) considering fracture planes uses the directional difference between two fracture planes. By projecting the line connecting the centers onto the planes, two included angles, ϕ_1 and ϕ_2 , between the projected line

and the connection line are measured. **b** Two methods for forming fracture shape: Formation (1) connects fracture centers denoted by “filled circles” to make a TIN, and Formation (2) produces a plane that consists of the averages of strikes and dips of the connectable facets. The “open circles” is a disk of a facet with its center at “asterisks” that projects a position “filled circles” onto the plane. The plane edge in the right figure is produced by enveloping the disks

Fig. 4 Arrangement of the petroleum storage tanks and tunnels in the Kikuma granite site on the Takanawa Peninsula, southwest Japan. The disks show the location of the fracture sample data, which were acquired basically from the sketch maps of the tank arches and tunnel floors. Locations in the study area are expressed using the forth plane rectangular coordinate system of Japan



different directions and positional offsets. An actual fracture is not as simple as having a shape following a plane. Two methods for forming the fracture shape were examined (Fig. 3b). Formation (1) connects fracture centers to make a TIN (triangulated irregular network). In Formation (2),

average of orientations of the connectable facets is calculated using their pole directions and a plane that has these averages is determined. The plane is then bounded to make a polygon by projecting the disks of the facets onto the plane and enveloping them.

Application to fracture modeling at a granite site

Study area and fracture sample data

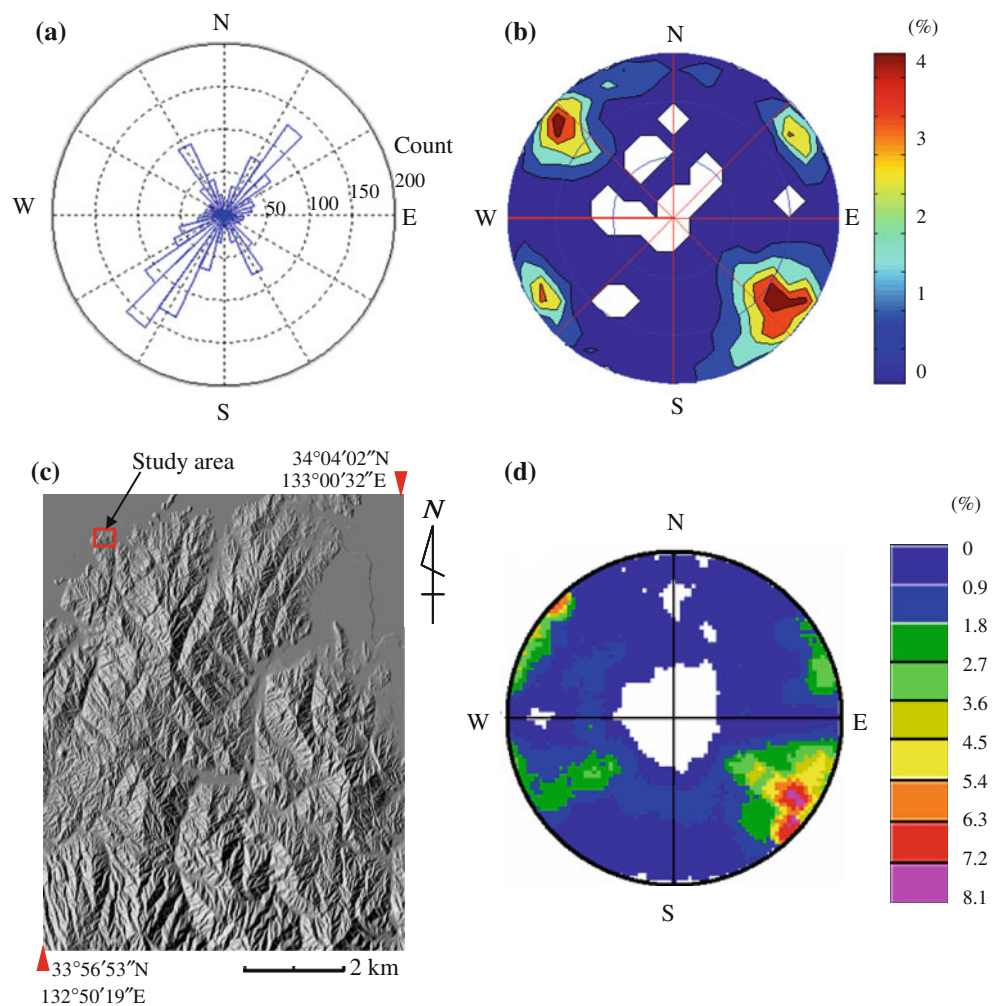
As a case study of applying GEOFRAC, the Kikuma granite site on the Takanawa Peninsula, southwest Japan (Fig. 4), was selected because the fractures were systematically measured during the construction of petroleum storage tanks. The Takanawa Peninsula is located 20 km north of the longest active fault in Japan (the Median Tectonic Line) and is almost underlain by Late Cretaceous granodiorite, termed Ryoke granite. The granite is intruded by aplite and pegmatite dykes in places.

A total of 1,843 fracture data were used from the walls of the tanks, sealing water tunnels, and connection tunnels of 5,025.4 m total length, located at three levels, -46 , -12 , and 4.4 m a.s.l. Long fractures crossing the arch walls of each tank and tunnel were selected. The minimum length of the fractures is around 10 m. The data at different levels are suitable for 3D fracture modeling. The petroleum storage tanks of 2,343 m total length are set at -46 m and along

$N54^{\circ}W$. At -12 m, there is a total of 1,707 m of tunnels composed of four sealing water tunnels that were set parallel to the tanks and three connection tunnels tending NW. One connection tunnel at 4.4 m has two main orthogonal segments: a shorter NW segment and a longer NE segment. In addition to these horizontally excavated tunnels, there is one 275 m sealing water tunnel in the middle dipping at 6.2° northward from -35 m. Figure 4 depicts the arrangement of the tunnels and the location of the fracture sample data which are viewed from different angles. The fracture sample data were acquired basically from the sketch maps of the tank arches and tunnel floors. The target space for 3D fracture modeling was limited to the domain including the tanks and tunnels, specifically 700 m E–W, 600 m N–S, and a 100 m depth from the ground surface.

Inevitably, fracture directions are controlled by the observation direction and the fractures perpendicular to this direction are preferably seen. As shown in Fig. 4, the tanks and tunnels tend mostly NW and are oriented horizontally, which means there is a dominance of NE striking fractures with steep dips. Figure 5a and b shows the frequencies of

Fig. 5 **a** Frequencies of strikes by the right hand rule in Fig. 1a and **b** the density distribution of poles of fracture planes using the lower hemisphere projection of Schmidt's net. Result of lineament analysis for extracting regional information on fractures in the 7×10 km area on the Takanawa Peninsula: **c** shaded DEM of 10 m interval, and **d** the density distribution of poles of the fracture planes interpreted from the DEM by the method of Koike et al. (1998) and Koike and Ichikawa (2006) (lower hemisphere projection of Schmidt's net)



strikes (α) by the above right hand rule and the density distribution of poles of fracture planes using the lower hemisphere projection of Schmidt’s net. They clarify that the NE strikes are predominant and orthogonal NW strikes are subordinate. The dips are mostly steep and are concentrated within the range 70–90°; NW dips are slightly present for the NE strikes, while NE and SW dips are almost the same as for the NW strikes. Such directional characteristics are in agreement with the predicted bias, but there is a possibility that this agreement is an apparent phenomenon.

To check this bias, a lineament analysis was adopted using a digital elevation model (DEM) dataset of high spatial resolution. Figure 5c depicts a shaded DEM of 10 m intervals covering the 7 × 10 km area of the Takanawa Peninsula. From the DEM, the directions of estimated continuous fracture planes were calculated as shown in Fig. 5d using the method proposed by Koike et al. (1998) and Koike and Ichikawa (2006), which is based on a vector analysis for the traces of extracted lineaments in the DEM. The density distribution of poles for the estimated fracture planes from the lineaments are highly in agreement with the fracture sample data.

In addition, fractures were observed in large spaces and were different from those of the small diameter borehole investigation; the tanks are 30 m high. Such large spaces can reveal fractures that are parallel to the tank axis and are dipping gently. Therefore, the fracture data can be regarded as representing the general characteristic in the granite and the directional bias may be small. A bias correction method was not applied to the fracture data based on that interpretation.

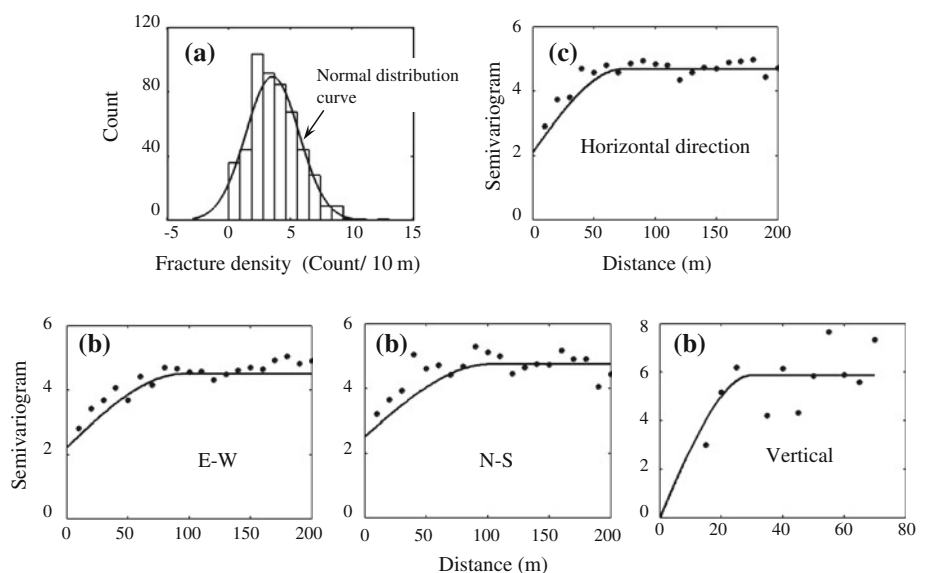
Spatial modeling of fracture density and orientation

The only way to define fracture density from the sketch map in this study is to use the number of fractures per unit

length along the tanks and tunnels. Therefore, a suitable selection of unit length is important as it must affect the appropriateness of the fracture modeling. Unit length determines the model resolution which captures the minimum scale of spatially correlated fractures. In addition, it depends on an interpretation of fractures, i.e., how the minimum size of fractures is assumed from the viewpoints of geological condition and sampling condition. In consideration of these aspects and also by checking the normality of the histogram and the clearness of the spatial correlation on the variogram of the fracture densities, the unit length was set at 10 m. Figure 6a shows the histogram of fracture density (number of fractures per 10 m) which roughly follows a normal distribution.

Figure 6b contains three directional $\gamma(h)$ s along E–W, N–S, and vertical paths; all can be approximated by a spherical model and the E–W and N–S $\gamma(h)$ s are almost identical. Thus, the omnidirectional $\gamma(h)$ was used along the horizontal direction (Fig. 6c) and geometric and zonal anisotropies of $\gamma(h)$ were assumed between the horizontal and vertical directions. The range in the horizontal $\gamma(h)$ is about 75 m, which can be interpreted as the typical dimension of fractures as discussed later. If the fracture data were sampled from boreholes, this could induce a strong bias in the semivariograms. This occurs because the fractures from the boreholes are indeed one dimensional data and have the strongest directional bias depending on the borehole direction. As described above, the present fracture data are not exactly one dimensional data. The data were sampled from the large tanks with relatively wide arches (longer than 10 m). Furthermore, the weakness of the directional bias was checked by a comparison with the lineament data as shown in Fig. 5d. Consequently, the bias in the semivariograms produced from the present fracture data must be small.

Fig. 6 Characterization of fracture density (number of fractures per 10 m) by **a** histogram, **b** three directional semivariograms along E–W, N–S, and vertical directions and their approximation by the spherical model, and **c** omnidirectional semivariogram along the horizontal direction



Based on the anisotropic $\gamma(h)$ model of the fracture density calculated with a 10 m interval, the fracture density distribution was simulated by SGS using the unit grid-cell size of $10 \times 10 \times 10$ m in accordance with the unit length for fracture density. Figure 1 (ESM only) presents examples of the fracture density map sliced at -5 , -35 , and -75 m a.s.l. The most remarkable characteristic is that the general trend of the density distribution is almost the same in spite of different elevations; the densities are commonly small in the northern and southeastern zones and are large on the southwestern and northeastern sides from the middle; and the locations of the largest densities, including relative densities larger than 4, do not change. The large density zones are isolated at shallow depths such as -5 m, but tend to be connected at deeper depths such as -35 and -75 m along NE and NW directions.

Fracture width is also an important attribute because the continuity of a fracture is related to width in general. The width data are low in confidence because most fractures are closed and the number of width data recorded is small; the histogram of the width data is skewed to small values as shown in Fig. 2a (ESM only). In spite of this, the omnidirectional experimental $\gamma(h)$ and its approximation by a spherical model using the log-transformed data in Fig. 2b (ESM only) suggest the existence of spatial correlation in the width.

For the indicator transformation of strikes and dips, the 8 and 16 divisions as shown in Fig. 2 were tried, but the 16 divisions were found not to be suitable for the above criterion, namely adequate decomposition of directional clouds and the small scattering in variography. Consequently, the 8 divisions were selected and the transformed binary sets were applied to the PCA. Figure 3 (ESM only) depicts the omnidirectional experimental $\gamma(h)$ s of the seven principal component values; although nugget effects occupy as much as about 50% of the sills, they can be approximated by a spherical model as shown by curves superimposed onto the graphs. An interesting feature is that the $\gamma(h)$ ranges of the first to fourth principal component values are similar to those of the horizontal fracture density (Fig. 6c) and the fracture width (Fig. 2b, ESM only). Estimation (OK) and simulation (SGS) methods are both available for spatial modeling of the principal component values of the fracture directions. Since the SGS generated fracture directions were too scattered, the OK was selected for modeling.

Results of simulation

By comparing the plausibility of the simulated fracture distributions constructed by the connection and shape forming criteria, the connection criterion (2) was chosen by assigning $\varphi_t = 5^\circ$ and $l_t = 70$ m, and the formation

method (2) was adopted. These values are derived empirically and therefore, must be changed depending on geology, location, properties of fractures, and measurement conditions of the fracture data; but the range of $\gamma(h)$ for the fracture density gives tentative criteria for l_t . While the formation method (1) is more exact in its fracture shape, the alternative (2) is more suitable for the graphic display of the long fracture planes. The diameter of the isolated fracture was defined as 10 m considering the unit grid-cell size.

Figure 4 (ESM only) shows the simulation result by GEOFRAC with the distributions of all fractures including isolated fractures, strikes, and pole directions. It is difficult to distinguish many simulated fractures by 2D graphics and thus each fracture was expressed by a semitransparent plane colored randomly. The fracture distributions are viewed vertically downward and the fractures approach lines with increasing dip angles. The simulated fractures are occupied by steep fractures with dip angles larger than 70° . Similar trends to the sample data appear in the GEOFRAC result except that the NW striking and NE dipping fractures are not predicted.

Figure 7a selects continuous fracture planes formed by more than four facets. Obviously the agreeable directional trends with the sample data are obtained by GEOFRAC, especially the trend that north dips are more frequent than south dips in the most dominant NE strikes.

Discussions

The effectiveness and plausibility of the 3D simulated fracture distributions by GEOFRAC are verified by the following four viewpoints.

Comparison with fracture zones

For the locations and distributions of continuous fractures to emerge, fracture planes formed from more than 20 facets are selected as drawn in Fig. 7b with the fracture zones inferred by the geological investigation during the storage tank constructions (Japan Underground Oil Storage Co., Ltd. 1991). Obviously, the NE striking fractures are much longer than the NW strikes and are concentrated in the northern zone.

It can be confirmed that all the fracture zones, numbered 1–4, appear as continuous GEOFRAC fractures. There are three noteworthy points in the GEOFRAC result. The first is that the slight bend of fracture zone 2 in the middle area, which is a change in the strike of 15° , can be followed by GEOFRAC. The second point is that the NW–SE connectivity, which corresponds with zones 3 and 4, can be reproduced from only a small amount of the NW striking

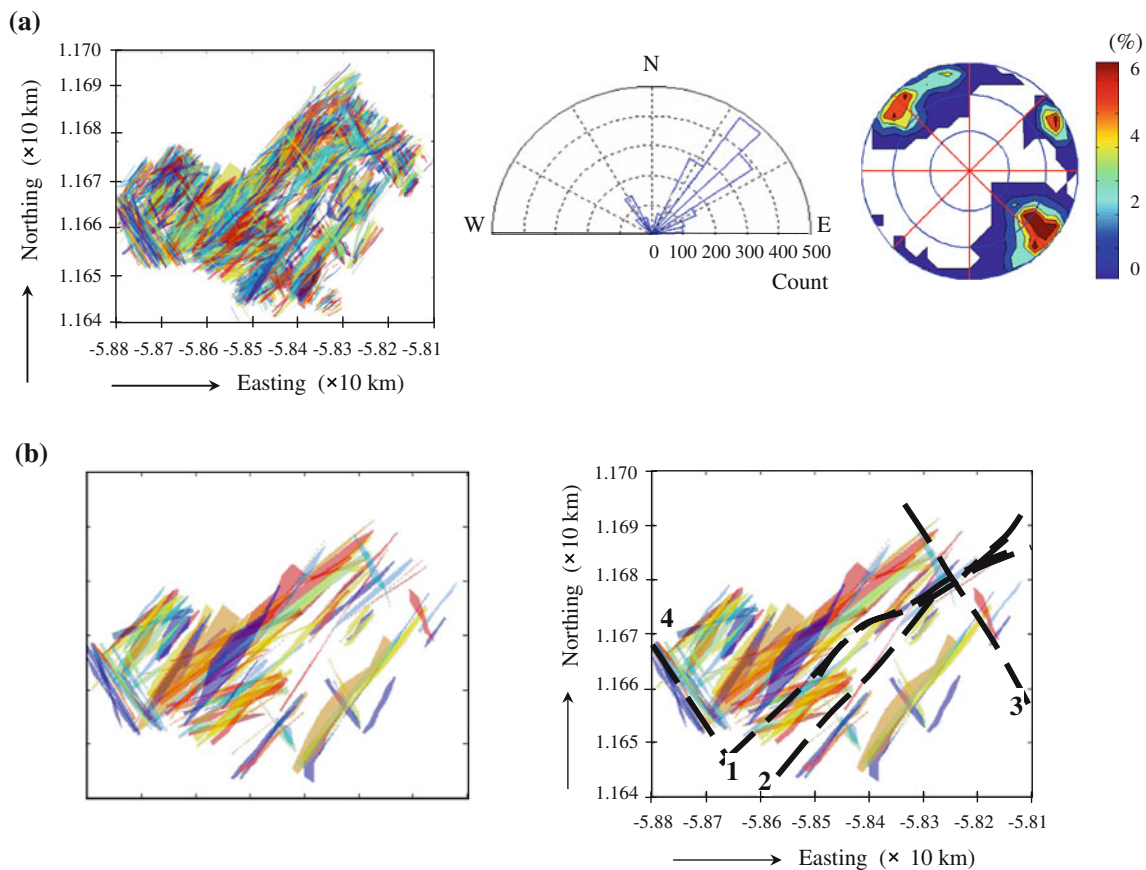


Fig. 7 **a** Selection of continuous fracture planes formed by more than four facets. Each fracture plane is expressed by a semitransparent plane colored randomly. The fracture distributions are viewed vertically downward and the fractures approach the lines with

increasing dip angles. **b** Comparison of distributions of continuous fractures forming more than 20 facets, with four fracture zones inferred by the geological investigation during the storage tank constructions

sample data. An interesting feature is seen in that several fractures parallel to zone 4 systematically exist around the zone. The third is that the continuous fractures are estimated in the zones with no sample data such as the NE fractures in contact with the southern edges of the tanks.

All the continuous NE striking fractures are not steep; there are small dip angles in the southern and northern areas. Figure 5 (ESM only) is a stereo-pair view of the GEOFRAC fractures in Fig. 7b that highlights the gentle dip fractures and connectivities of the fractures along the depth direction.

Effect of directional correction

Although the directional trends of the GEOFRAC fractures are in agreement with the sample data, the possibility that the strikes and dips of the data are biased strongly by the tank direction (NW–SE) cannot be denied. The bias correction may not be easy in most cases, because three unknown parameters must be defined: (1) the number of unmeasurable fractures (almost parallel to the measurement direction), which requires to estimate true population

of fracture orientations, (2) the locations of unmeasurable fractures for suitable variography, and (3) the correction weights depending on direction to increase the number of present fracture data. These definitions need many assumptions.

As an attempt to decrease the bias, a simple correction coefficient is used:

$$w = \frac{1}{\cos(\theta/2)} \tag{2}$$

where θ is the deviation angle from the NE–SW or SW–NE ($\alpha = 45^\circ$ or 225°), the strike that can appear most easily because it is perpendicular to the tank direction. This type of correction is the most traditional, which has been used widely (e.g., Terzaghi 1965; Laslett 1982). The value w is multiplied with the value in the corresponding directional interval, one of the back-transformed indicator set, (g_1, g_2, \dots, g_8) . This correction is expected to increase the possibility that strike directions except for NE are selected.

Figure 6 (ESM only) shows the GEOFRAC fractures with the directional correction, which are composed of more than four facets. The connection criteria are the same

as for the result without the correction in Fig. 7a. In fact, the correction can increase the appearance frequency of the NW striking fractures. However, it has negative effects in that the blank zones without continuous fractures become wide; the most dominant direction is deviated and the numbers of the most continuous NE striking fractures that penetrate the study area decrease. Therefore, the effect of the directional correction is not confirmed in the present case study, and the above assumption of the weakness of the directional bias may be correct.

Length distribution

A merit of fracture simulation is that it can contribute to estimating the fracture length distribution, because this estimation is impossible from the spatially isolated fracture data observed in tunnels and boreholes. Figure 8a presents a histogram of the length frequencies of the GEOFRAC fractures and their CDF. The histogram seems to follow the lognormal distribution that is used widely to approximate fracture lengths (e.g., Rouleau and Gale 1985). The CDF curve clarifies interesting characteristics in that the CDF increases linearly until 75 m and the increase ratio becomes gentle in the longer region, but there is another inflection point at 130 m. Using the CDF, the median length of the fractures can be estimated as 40 m.

The value 75 m should be related to the connection threshold, l_c . However, the ranges in the $\gamma(h)$ s are similar, hence 75 m may have some tectonic meaning. Based on this assumption, the fractures can be classified into three categories by length: (1) 0–75 m, (2) 75–130 m, and (3) longer than 130 m. The maximum length of one category can be interpreted as limiting a correlation length (range) found by variography. Nureki (1958) considered the main fractures in the granite in the Takanawa Peninsula were probably caused by cooling joints. Predominant small fractures of category (1), which account for 85% of the total simulated fractures, may be cooling joints. On the contrary, a large fracture of category (3) may have been caused under the regional tectonic stress field. The existence of the fracture zone (Fig. 7b) and the lineament data (Fig. 5d) support this interpretation.

Application to hydraulic characterization

As examined by Koike and Ichikawa (2006), the simulated fractures can be linked by permeability tensor analysis to characterize the hydraulic property of the study area from the viewpoints of major directions and dimensions, expressed by permeability or hydraulic conductivity, of fluid flows. Details on calculating the permeability tensor are given in the Appendix.

Fig. 8 a Histogram of length frequencies of the GEOFRAC fractures and their CDF. **b** Histogram and the CDF of the hydraulic conductivity data obtained by the hydraulic well tests at 15 sites in the study area

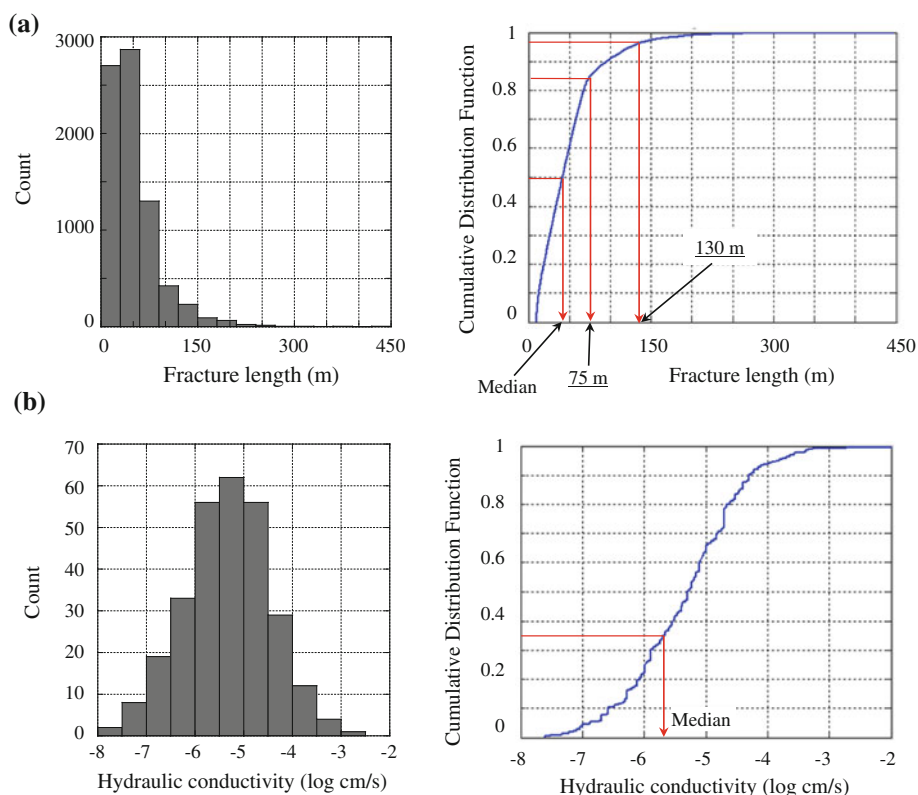


Table 1 Calculated permeability (m^2) along the first, second, and third principal axes and the directions of the axes by combining the GEOFRAC fractures with the permeability tensor analysis. The permeability is transformed roughly into hydraulic conductivity (cm/s) by multiplying by 10^9

Parameters	1st axis	2nd axis	3rd axis
Permeability ($\times 10^{-15} m^2, mD$)	8	7.8	1
Hydraulic conductivity ($\times 10^{-5} cm/s$)	0.80	0.78	0.10
Direction	S43°E	N47°E	N43°W
Dip	88°	0	2°

Table 1 shows the calculated permeability (m^2) along the first, second, and third principal axes and the directions of the axes. These are equivalent permeability of the fracture system. The permeability can be transformed roughly into hydraulic conductivity (cm/s) by multiplying by 10^9 . The first axis pointing toward S43°E with 88° dip and the second axis horizontally toward N47°E correspond with the flows along the dip and strike directions, respectively, of the N47°E striking and N88°W dipping plane. Both flows are related to the dominant fractures. The third axis is the horizontal flow along the strike N43°W of the second dominant fracture.

Figure 8b shows the histogram and CDF of the hydraulic conductivity data obtained by the hydraulic well tests at 15 sites in the study area. They are concentrated in the range from 10^{-6} to 10^{-4} cm/s with the median 0.2×10^{-5} cm/s. The calculated hydraulic conductivities are 0.80×10^{-5} , 0.78×10^{-5} , and 0.10×10^{-5} cm/s along the first, second, and third principal axes, respectively. The first two values are almost the same, which shows the strong effect of the NE striking fractures on the fluid flows. It is noteworthy that the order of the calculated hydraulic conductivities, 10^{-5} cm/s, coincides with that of the representative value of the measured data. This comparison between the measurement and calculation is not precise because the hydraulic conductivity data by well tests must be affected by various fracture properties. Nevertheless, the representative value of the measured data is probably related to major fractures. The coincidence can be considered to demonstrate the usefulness of GEOFRAC and the propriety of the simulated fractures.

Conclusion

In this paper, a 3D simulation method for the fracture distribution that considers strikes and dips, GEOFRAC, was proposed and the simulated fractures were validated from several viewpoints. GEOFRAC was composed of three steps: positioning of fracture centers using the fracture density data by sequential Gaussian simulation,

assignments of directions (strikes and dips), and connection of facets for forming a plane. The main results obtained are summarized:

1. For calculating fracture directions, GEOFRAC applied a transformation of the sample direction data into an indicator set and principal component analysis to compress the data set and construct semivariograms of principal components. From a case study for the petroleum storage stations in the Kikuma granite area, the directional trends of the GEOFRAC fractures agreed with those of the fracture sample data and the more regional characteristics due to the lineaments derived from the shaded DEM using a 10 m interval.
2. All the fracture zones appeared as continuous GEOFRAC fractures. The capability of GEOFRAC was confirmed on three counts: the reproduction of a slight bend of a fracture zone, the estimation of the NW–SE connectivity from only a small number of NW striking sample data; and the simulation of continuous fractures in zones with no sample data.
3. The length frequencies of the GEOFRAC fractures suggest an estimation of the median length of 40 m. A large inflection point at 75 m may have some tectonic meaning, because the ranges found in the variography are similar. The length frequencies can be used to classify the fractures by their generation mechanism such as a cooling joint or a small fault.
4. By combining the GEOFRAC fractures with permeability tensor analysis, the strong effect of the dominant NE striking fractures on the fluid flows was confirmed; the flows along the fractures were estimated to be eight times the conductivity of those along the second dominant NW striking fractures. The usefulness of GEOFRAC was demonstrated by the coincidence of the orders of the calculated hydraulic conductivities, 10^{-5} cm/s, with that of the representative value of the measured data.

Acknowledgments The authors express their sincere thanks to Japan Underground Oil Storage Co., Ltd., for providing the valuable investigation data at Kikuma Station, and to Dr. Alaa A. Masoud of Tanta University for his cooperation with the lineament analysis using the shaded DEM. Sincere thanks are also extended to the Japan Society for the Promotion of Science (JSPS) and Project 40902058 of National Natural Science Foundation of China (NSFC) for supporting research activities of the second author, and anonymous reviewers for their valuable comments and suggestions.

Appendix: calculation of the permeability tensor

Following Oda et al. (1987), the three dimensional permeability tensor, k_{ij} , is expressed by

$$\mathbf{k}_{ij} = \eta(\mathbf{P}_{kk}\delta_{ij} - \mathbf{P}_{ij})$$

$$\mathbf{P}_{ij} = \frac{\pi\rho}{4} \int_0^\infty \int_0^\infty \int_\Omega r^2 t^3 \mathbf{n}_i \mathbf{n}_j E(\mathbf{n}, r, t) d\Omega dr dt \quad (\text{A.1})$$

where δ_{ij} is a delta function, η is a constant expressing the continuity of fractures, r is the diameter of the fracture, t is the hydraulic aperture of the fracture, \mathbf{n} is a normal vector of the fracture plane formed by the connection criteria, $E(\mathbf{n}, r, t)$ is the probabilistic density function with respect to \mathbf{n} , r , and t , ρ is the volumetric fracture density, and Ω is a solid angle.

\mathbf{P}_{ij} can be transformed to a discrete expression as

$$\mathbf{P}_{ij} = \frac{1}{V} \sum_{k=1}^K r_k [t_k^3] n_{ik} n_{jk} \quad (\text{A.2})$$

where V is the volume of the study region and K is the number of fracture planes. Assuming the fracture shape is a plate (i.e., t is constant for one fracture plane), then η is defined as $1/12$. r is defined by the diameter of the equivalent circle that has the same area as the fracture plane.

Although t is a crucial parameter for controlling the order of the calculated permeability, it cannot be determined uniquely. Following the examination by Koike and Ichikawa (2006), t was supposed as r multiplied by 10^{-6} .

References

- Acuna J, Yortsos Y (1995) Application of fractal geometry to the study of networks of fractures and their pressure transient. *Water Resour Res* 31:527–540
- Andersson J, Dverström B (1987) Conditional simulations of fluid flow in three-dimensional network of discrete fractures. *Water Resour Res* 23:1876–1886
- Andersson J, Thunvik R (1986) Predicting mass transport in discrete fracture networks with the aid of geometrical field data. *Water Resour Res* 22:1941–1950
- Andersson J, Shapiro AM, Bear J (1984) A stochastic model of a fractured rock conditioned by measured information. *Water Resour Res* 20:79–88
- Billaux D, Chilès JP, Hestir K, Long J (1989) Three-dimensional statistical modelling of a fractured rock mass—an example from the Fanay-Augères mine. *Int J Rock Mech Miner Sci and Geomech Abstr* 26:281–299
- Cacas MC, Ledoux E, DeMarsily G, Tille B, Barbreau A, Durand E, Feuga B, Peaudecerf P (1990) Modelling fracture flow with a stochastic discrete fracture network: calibration and validation: 1. The flow model. *Water Resour Res* 26:479–489
- Chilès JP (1988) Fractal and geostatistical methods for modeling of a fracture network. *Math Geol* 20:631–654
- Clemo T, Smith L (1997) A hierarchical model for solute transport in fractured media. *Water Resour Res* 33:1763–1783
- Dershowitz WS, Einstein HH (1988) Characterizing rock joint geometry with joint system models. *Rock Mech and Rock Eng* 21:21–51
- Deutsch CV, Journel AG (1998) GSLIB: Geostatistical software library and user's guide. Oxford University Press, London
- Heffer KJ, Bevan TG (1990) Scaling relationships in natural fractures: data, theory, and application. In: Proceedings of the 2nd European Petroleum Conference, pp 367–376
- Hewett TA (1994) Fractal methods for fracture characterization. In: Yarus JM, Chambers RL (eds) Stochastic modeling and geostatistics: principles, methods, and case studies. AAPG Compute Applications in Geology 3, AAPG, pp 249–260
- Japan Underground Oil Storage Co. Ltd. (1991) Report on Enforcement Management Work of the Kikuma Station Construction-Geological Series (in Japanese)
- Koike K, Ichikawa Y (2006) Spatial correlation structures of fracture systems for identifying a scaling law and modeling fracture distributions. *Comput Geosci* 32:1079–1095
- Koike K, Nagano S, Kawaba K (1998) Construction and analysis of interpreted fracture planes through combination of satellite-image derived lineaments and digital elevation model data. *Comput Geosci* 24:573–583
- Koike K, Komorida K, Ichikawa Y (2001) Fracture-distribution modeling in rock mass using borehole data and geostatistical simulation. In: Proceedings of International Association for Mathematical Geology Conference (Cancun 2001), CD-ROM
- Laslett GM (1982) Censoring and edge effects in areal and line transect sampling of rock joint traces. *Math Geol* 14:125–140
- Long JCS, Billaux DM (1987) From field data to fracture network modeling: an example incorporating spatial structure. *Water Resour Res* 23:1201–1216
- Long JCS, Gilmour P, Witherspoon PA (1985) A model for steady fluid flow in random three-dimensional networks of disc-shaped fractures. *Water Resour Res* 21:1105–1115
- Mauldon M, Dunne WM, Rohrbach MB Jr (2001) Circular scanlines and circular windows: new tools for characterizing the geometry of fracture traces. *J Struct Geol* 23:247–258
- Nureki T (1958) On the structure of granite complex in the northern part of the Takanawa Peninsula, Ehime prefecture. *J Sci of the Hiroshima Univ (Ser. C, Geol and Mineral)* 2:109–127
- Oda M, Hatsuyama Y, Ohnishi Y (1987) Numerical experiments on permeability tensor and its application to jointed granite at Stripa mine, Sweden. *J Geophys Res* 92B:8037–8048
- Odling NE (1997) Scaling and connectivity of joint systems in sandstones from western Norway. *J Struct Geol* 19:1257–1271
- Priest SD, Hudson JA (1976) Discontinuity spacings in rock. *Int J Rock Mech Min Sci and Geomech Abstr* 13:135–148
- Riley MS (2004) An algorithm for generating rock fracture patterns: mathematical analysis. *Math Geol* 36:683–702
- Rouleau A, Gale JE (1985) Statistical characterization of the fracture system in the Stripa granite, Sweden. *Int J Rock Mech Min Sci and Geomech Abstr* 22:353–367
- Rouleau A, Gale JE (1987) Stochastic discrete fracture simulation of groundwater flow into an underground excavation in granite. *Int J Rock Mech Min Sci and Geomech Abstr* 24:99–112
- Snow DT (1969) Anisotropic permeability of fractured media. *Water Resour Res* 5:1273–1289
- Suro-Pérez V, Journel AG (1991) Indicator principal component kriging. *Math Geol* 23:759–788
- Terzaghi RD (1965) Sources of error in joint surveys. *Geotech* 15:287–304
- Tran NH, Chen Z, Rahman SS (2006) Integrated conditional global optimisation for discrete fracture network modeling. *Comput Geosci* 32:17–27